DOI: 10.1021/ic9014114

Inorganic Chemistry
Article

Electrochemical and Chemical Reduction of Disulfur Dinitride: Formation of $[S_4N_4]^{-\bullet}$, EPR Spectroscopic Characterization of the $[S_2N_2H]^{\bullet}$ Radical, and X-ray Structure of [Na(15-crown-5)][S_3N_3]

Tracey L. Roemmele,[†] Jari Konu,[‡] René T. Boeré,*[,†] and Tristram Chivers*[,‡]

[†]*Department of Chemistry and Biochemistry, University of Lethbridge, Lethbridge, Alberta, Canada T1K 3M4, and* [‡]*Department of Chemistry, University of Calgary, Calgary, Alberta, Canada T2N 1N4.*

Received July 19, 2009

Voltammetric studies of S_2N_2 employing both cyclic voltammetry (CV) and rotating disk electrode (RDE) methods on GC electrodes at room temperature (RT) revealed two irreversible reduction processes at about −1.4 V and −2.2 V in CH_3CN, CH_2Cl_2, and tetrahydrofuran (vs ferrocene) and no observable oxidation processes up to the solvent limit when the scan is initially anodic. However, after cycling the potential through −1.4 V, two new couples appear near −0.3 V and −1.0 V due to $[S_3N_3]^{-/0}$ and $[S_4N_4]^{-/0}$ respectively. The diffusion coefficient D for S_2N_2 was determined to be 9.13×10^{-6} cm^2 s^{-1} in CH_2Cl_2 and 7.65×10^{-6} cm^2 s^{-1} in CH_3CN. Digital modeling of CVs fits well to a mechanism in which $[S_2N_2]^{-\bullet}$ couples rapidly with S_2N_2 to form $[S_4N_4]^{-\bullet}$, which then decomposes to $[S_3N_3]^-$. In situ electron paramagnetic resonance (EPR) spectroelectrochemical studies of S_2N_2 in both CH_2Cl_2 and CH_3CN resulted in the detection of strong EPR signals from $[S_4N_4]^{-\bullet}$ when electrolysis is conducted at −1.4 V; at more negative voltages, spectra from transient adsorbed radicals are observed. In moist solvent or with added HBF_4, a longer-lived spectrum is obtained due to the neutral radical $[S_2N_2H]^{\bullet}$, identified by simulation of the EPR spectrum and density functional theory (DFT) calculations. The chemical reduction of S_2N_2 with Na[$C_{10}H_8$] or Na[Ph_2CO] produces [Na(15-crown-5)][S_3N_3], while reduction with cobaltocene gives [Cp_2Co][S_3N_3]. The X-ray structure of the former reveals a strong interaction (Na···N = 2.388(5) Å) between the crown ether-encapsulated Na^+ cation and one of the nitrogen atoms of the essentially planar six-membered cyclic anion $[S_3N_3]^-$.

Introduction

The binary sulfur nitride S_2N_2 has been known for more than 50 years.[1] It is commonly prepared by the thermolysis of the cage molecule S_4N_4 over silver wool at about 220 °C,[2] although other sulfur−nitrogen rings, for example, $[S_4N_3]Cl$[3] and $Ph_3As{=}N{-}S_3N_3$[4] have been used as a source of S_2N_2. Disulfur dinitride has a square-planar structure with S−N bond distances intermediate between single-and double-bond values.[2] The four-membered ring is an important precursor for the synthesis of the conducting polymer poly(sulfur nitride) $(SN)_x$.[5] In this solid-state polymerization which occurs at 0 °C over several days, colorless crystals of S_2N_2 are converted via a topochemical process into shiny bronze-colored fibers of $(SN)_x$. Recent work by Kelly et al. has shown that this polymerization process can be effected in a zeolitic matrix.[6] In an intriguing contribution the same group has shown that the $S_2N_2 \rightarrow (SN)_x$ conversion is a potential device for latent fingerprint detection.[7]

The electronic structure of this compositionally simple heterocycle continues to be a matter of debate.[8] Simple electron-counting procedures lead to the conclusion that S_2N_2 is a six π-electron (aromatic) system.[9] However, four

*To whom correspondence should be addressed. E-mail: boere@uleth.ca (R.T.B.), chivers@ucalgary.ca (T.C.). Phone: (403) 329-2045 (R.T.B.), (403) 220-5741 (T.C.). Fax: (403) 329-2057 (R.T.B.), (403) 289-9488 (T.C.).

(1) (a) Goehring, M.; Voigt, D. *Naturwissenschaften* **1953**, *40*, 481. (b) Goehring, M.; Voigt, D. *Z. Anorg. Allg. Chem.* **1956**, *285*, 181.
(2) Mikulski, C. M.; Russo, P. J.; Sorna, M. S.; MacDiarmid, A. G.; Garito, A. F.; Heeger, A. J. *J. Am. Chem. Soc.* **1975**, *97*, 6358.
(3) Banister, A. J.; Hauptman, Z. V. *J. Chem. Soc., Dalton Trans.* **1980**, 731.
(4) Chivers, T.; Cordes, A. W.; Oakley, R. T.; Swepston, P. N. *Inorg. Chem.* **1981**, *20*, 2376.
(5) Cohen, M. J.; Garito, A. F.; Heeger, A. J.; MacDiarmid, A. G.; Mikulski, C. M.; Saran, M. S.; Kleppinger, J. *J. Am. Chem. Soc.* **1976**, *98*, 3844.
(6) King, R. S. P.; Kelly, P. F.; Dann, S. E.; Mortimer, R. J. *Chem. Commun.* **2007**, 4812.
(7) Kelly, P. F.; King, R. S. P.; Mortimer, R. J. *Chem. Commun.* **2008**, 6111.
(8) (a) Gerratt, J.; McNicholas, S. J.; Karadakov, P. B.; Sironi, M.; Raimondi, M.; Cooper, D. L. *J. Am. Chem. Soc.* **1996**, *118*, 6472. (b) Mawhinney, R. C.; Goddard, J. D. *Inorg. Chem.* **2003**, *42*, 6323. (c) De Proft, F.; Fowler, P. W.; Havenith, R. W. A.; Schleyer, P.v. R.; Van Lier, G.; Geerlings, P. *Chem.—Eur. J.* **2004**, *10*, 940. (d) Jung, Y.; Heine, T.; Schleyer, P. v. R.; Head-Gordon, M. *J. Am. Chem. Soc.* **2004**, *126*, 3132. (e) Tuononen, H. M.; Suontamo, R.; Valkonen, J.; Laitinen, R. S. *J. Phys. Chem. A* **2004**, *108*, 5670. (f) Tuononen, H. M.; Suontamo, R.; Valkonen, J.; Laitinen, R. S.; Chivers, T. *J. Phys. Chem. A* **2005**, *109*, 6309. (g) Klein, H.-P.; Oakley, R. T.; Michl, J. *Inorg. Chem.* **1986**, *25*, 3194. (h) Gimarc, B. *Pure Appl. Chem.* **1990**, *62*, 423.
(9) (a) Chivers, T. *A Guide to Chalcogen-Nitrogen Chemistry*; World Scientific Publishing Co.: Singapore, 2005. (b) Greenwood, N. N.; Earnshaw, A. *Chemistry of the Elements*; 2nd ed.; Butterworth-Heinemann: Oxford, U.K., 1997; pp 721−726.

Published on Web 08/28/2009

of the six π-electrons occupy non-bonding π MOs (i.e., those with nodes either through both sulfur or both nitrogen atoms). S_2N_2 is more appropriately considered as a two π-hole $(4N + 2)$-electron system[8g,h] with minor singlet diradical character (ca. 6%), which is attributed solely to the nitrogen atoms.[8d−f]

Apart from polymerization, investigations of the reactions of S_2N_2 have been limited. The four-membered ring forms *N*-bonded mono and diadducts of the type $S_2N_2 \cdot L$ and $S_2N_2 \cdot 2L$ with a variety of Lewis acids, for example, $AlCl_3$,[10] $SbCl_5$,[11] and with transition-metal halides.[12] In the presence of trace amounts of nucleophiles or reducing agents S_2N_2 dimerizes rapidly to S_4N_4,[13] but this process is not well understood. It has been suggested that it may involve the initial formation of the radical anion $[S_2N_2]^{-\bullet}$.[14] The interaction of the singly occupied molecular orbital (SOMO) of the radical anion with the lowest unoccupied molecular orbital (LUMO) of a neutral S_2N_2 molecule would produce an adduct that could readily isomerize to the tetrasulfur tetranitride radical anion $[S_4N_4]^{-\bullet}$ (Figure 1a). Density functional theory (DFT) calculations forecast that the D_{2d} cage of neutral S_4N_4 unfolds to a C_{2v} structure in which one of the transannular S···S bonds opens up more than the other (Figure 1b) while the four nitrogen atoms remain equivalent, upon addition of an electron to form the radical anion $[S_4N_4]^{-\bullet}$.[15]

There have been no detailed studies of the electrochemistry of S_2N_2,[16] however DFT calculations for the radical anion $[S_2N_2]^{-\bullet}$ predict a square planar (D_{2h}) structure with bond lengths about 0.06 Å longer than those in the neutral molecule S_2N_2, as expected for population of the antibonding π-MO by a single electron.[15] Numerous metal complexes of the chelating acyclic dianion $[SNSN]^{2-}$ are known.[17] Two methods for the in situ generation of this ligand are (a) the reaction of $[S_4N_3]Cl$ with liquid ammonia[18] or (b) the deprotonation of the tetraimide $S_4(NH)_4$ in the presence of a base.[19] Weak NMR resonances observed for reaction (a) have been tentatively attributed to $[SNSN]^{2-}$.[18] The protonated monoanion $[S_2N_2H]^-$ has been convincingly shown to be formed by deprotonation of 99% ^{15}N-enriched $S_4(NH)_4$ with KNH_2 in liquid ammonia solutions using ^{15}N NMR

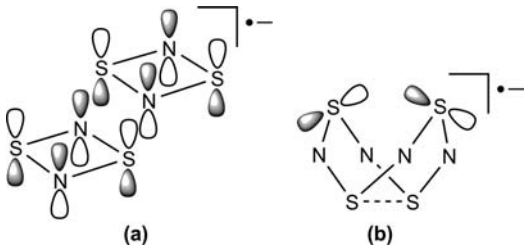

Figure 1. (a) Interaction between the LUMO of S_2N_2 and the SOMO of $[S_2N_2]^{-\bullet}$, and (b) the SOMO of the C_{2v} symmetric $[S_4N_4]^{-\bullet}$ radical anion.

spectroscopy.[20] However, attempts to detect the formation of dianion $[S_2N_2]^{2-}$ via reaction (b) by this technique were unsuccessful.[20a]

In recent publications we applied modern electrochemical and electron paramagnetic resonance (EPR) methods to redox reactions of S,N heterocycles[21] and binary sulfur nitrides.[22] In the latter contribution simultaneous electrochemical EPR (SEEPR) spectroscopy was used to provide a comprehensive characterization of the $[S_4N_4]^{-\bullet}$ radical anion.[22] Kinetic models for the conversion of S_4N_4 to $[S_3N_3]^-$ upon one-electron reduction and for the reverse process upon oxidation were also developed. We have now carried out the first thorough voltammetric studies of S_2N_2 and have determined the identity of the redox products, including the neutral radical $[S_2N_2H]^{\bullet}$ formed by proton transfer[23] by using SEEPR spectroscopy in conjunction with DFT calculations. Digital modeling of CVs has been applied to determine the pathway for this transformation. Finally, we have identified the products of the chemical reduction of S_2N_2 with cobaltocene Cp_2Co, sodium naphthalenide $[Na][C_{10}H_8]$, and sodium benzophenone $[Na][Ph_2CO]$, and report details of the X-ray structure of $[Na(15\text{-crown-}5)][S_3N_3]$.

Experimental Section

Caution! *In the pure form both S_4N_4 and S_2N_2 are friction-sensitive explosives.[9] The latter has been reported to spontaneously detonate above 30 °C, although we have not encountered such instability. All the appropriate safety precautions must be observed in their handling.*

General Procedures. The reactions with S_2N_2 and the manipulations of products were performed under an argon atmosphere by using standard Schlenk techniques or an inert atmosphere glovebox. The starting materials S_4N_4[24] and S_2N_2[2] were prepared by following the literature methods, and they were purified by recrystallization from CH_3CN and Et_2O, respectively. Isotopically labeled $S_2{}^{15}N_2$ was prepared from 99% $S_4{}^{15}N_4$.[22] The solvents Et_2O and tetrahydrofuran (THF) were dried by distillation over Na/benzophenone, and the solvents CH_2Cl_2 and CH_3CN were distilled from CaH_2 under an argon atmosphere prior to use. Electrochemical grade tetrabutylammonium hexafluorophosphate $[^nBu_4N][PF_6]$ (Fluka) was used

(10) Patton, R. L.; Raymond, K. N. *Inorg. Chem.* **1969**, *8*, 2426.
(11) Thewalt, U.; Burger, M. *Angew. Chem., Int. Ed. Engl.* **1982**, *21*, 634.
(12) Dehnicke, K.; Muller, U. *Transition Met. Chem.* **1985**, *10*, 361.
(13) Becke-Goehring, M. *Inorg. Synth.* **1960**, *6*, 123.
(14) (a) Oakley, R. T. *Prog. Inorg. Chem.* **1988**, *36*, 299. (b) Bestari, K.; Oakley, R. T. *Can. J. Chem.* **1991**, *69*, 94.
(15) Boeré, R. T.; Tuononen, H. M.; Chivers, T.; Roemmele, T. L. *J. Organomet. Chem.* **2007**, *692*, 2683.
(16) To our knowledge, there is only one prior literature report of a voltammetric study of S_2N_2. In a paper that deals with the electrochemical reduction of the $[S_5N_5]^+$ cation it is reported that "$E_{p/2}{}^{red} = -0.85$ V, $E_{p/2}{}^{ox} = 0.1$ V (vs aq. SCE); S_2N_2 (*ca.* 10^{-3} mol dm^{-3}), $[NBu_4][BF_4]$ (0.1 mol dm^{-3}) in MeCN at 16.5°C". No further details are provided. Banister, A. J.; Hauptman, Z. V.; Kendrick, A. G.; Small, R. W. H. *J. Chem. Soc., Dalton Trans.* **1987**, 915.
(17) (a) Chivers, T.; Edelmann, F. *Polyhedron* **1986**, *5*, 1661. (b) Kelly, P. F.; Woollins, J. D. *Polyhedron* **1986**, *5*, 607.
(18) (a) Belton, P. S.; Parkin, I. P.; Williams, D. J.; Woollins, J. D. *J. Chem. Soc., Chem. Commun.* **1988**, 1479. (b) Parkin, I. P.; Woollins, J. D.; Belton, P. S. *J. Chem. Soc., Dalton Trans.* **1990**, 511.
(19) (a) Jones, R.; Kelly, P. F.; Warrens, C. P.; Williams, D. J.; Woollins, J. D. *J. Chem. Soc., Chem. Commun.* **1986**, 711. (b) Jones, R.; Kelly, P. F.; Williams, D. J.; Woollins, J. D. *Polyhedron* **1987**, *6*, 1541. (c) Chivers, T.; Edelmann, F.; Behrens, U.; Drews, R. *Inorg. Chim. Acta* **1986**, *116*, 1509.
(20) (a) Chivers, T.; Schmidt, K. J. *Can. J. Chem.* **1992**, *70*, 710. (b) Chivers, T.; Schmidt, K. J. *J. Chem. Soc. Chem. Commun.* **1990**, 1342.
(21) Boeré, R. T.; Bond, A. M.; Chivers, T.; Feldberg, S. W.; Roemmele, T. L. *Inorg. Chem.* **2007**, *46*, 5596.
(22) Boeré, R. T.; Chivers, T.; Roemmele, T. L.; Tuononen, H. M. *Inorg. Chem.* **2009**, *48*, 7294.
(23) Proton transfer to radical anions is documented in the literature, and when it results in a longer-lived radical is arguably a form of spin-trapping. (a) Funston, A. M.; Lymar, S. V.; Saunders-Price, B.; Czapski, G.; Miller, J. R. *J. Phys. Chem. B* **2007**, *111*, 6895. (b) Croft, A. K.; Lindsay, K. B.; Renaud, P.; Skrydstrup, T. *Chimia* **2008**, *62*, 735. (c) Rehorek, D. *Chem. Soc. Rev.* **1991**, *20*, 341.
(24) (a) Villena-Blanco, M.; Jolly, W. L. *Inorg. Synth.* **1967**, *9*, 98. (b) Maaninen, A.; Siivari, J.; Laitinen, R. S.; Chivers, T. *Inorg. Synth.* **2002**, *33*, 196.

as the supporting electrolyte and was kept in a desiccator prior to use. Ferrocene (Fc) was sublimed prior to use.

Electrochemical Procedures. Voltammetry, SEEPR, digital simulations, and bulk electrolysis experiments were conducted as in our previous study using the same apparatus, electrodes, and so forth except as noted below.[22] Voltammograms were obtained at 20 ± 2 °C in CH_3CN, CH_2Cl_2, and THF solutions containing 0.1 M, 0.4 M, and 0.4 M [^{n}Bu$_4$N][PF_6], respectively, as the supporting electrolyte. Cyclic voltammetry (CV) and rotating disk electrode (RDE) measurements were performed with a Bio-Analytical Systems (BASi) CV-50 computer-controlled potentiostat in conjunction with a PINE Model AFMSRXE Modulated Speed Rotator. The potentials for S_2N_2 are reported versus the operative formal potential, $E^{0/}_{Fc^{0/+}}$, for the $Fc^{0/+}$ redox couple, which was used as an internal standard, and literature data reported against SCE in CH_3CN/[^{n}Bu$_4$N][PF_6] have been converted to the Fc scale by subtraction of 0.38 V.[25] In situ EPR experiments (Bruker EMX 113 spectrometer, 9.8 GHz) were conducted on CH_2Cl_2 solutions of S_2N_2 at temperatures between −90 and −20 °C using the miniature solution cell described previously and in CH_3CN solutions down to −35 °C.[21,22] Experimental g values were determined with reference to external, solid DPPH (2.0037 ± 0.0002).[26] Simulations of EPR spectra were performed with Bruker Simfonia (version 1.25) and WinSim (version 0.98, 2002) software.[27] Computed cyclic voltammograms were produced using DigiElch software (www.elchsoft.de).[28]

Quantum Calculations. DFT calculations undertaken for this study employed geometry optimization at the (U)B3LYP/6-31G(d,p) level. Harmonic vibrational frequencies were calculated for all optimized geometries to confirm that they are stationary points. Calculation of energies and EPR hyperfine splitting (hfs) constants used (U)B3LYP/6-311G++(3df,3pd). All calculations were performed with the Gaussian 03 suite of programs.[29]

X-ray Crystallography. A yellow, plate-shaped crystal of [Na(15-crown-5)][S_3N_3] (**1a**) was coated with Paratone 8277 oil and mounted on a glass fiber. Diffraction data were collected on a Nonius KappaCCD diffractometer using monochromated MoK_α radiation (λ = 0.71073 Å) at −100 °C. The data were corrected for Lorentz and polarization effects, and an empirical absorption correction was applied to the net intensities. The structure was solved by direct methods using SHELXS-97[30] and refined using SHELXL-97.[31] After the full-matrix least-squares refinement of the non-hydrogen atoms with anisotropic thermal parameters, the hydrogen atoms were placed in calculated positions (C−H = 0.99 Å). The isotropic thermal parameters of the hydrogen atoms were fixed at 1.2 times to that of the corresponding carbon. In the final refinement the hydrogen atoms were riding on their respective carbon atoms. One of the oxygen atoms in the 15-crown-5 unit showed positional disorder with site occupancy factors of about 0.5:0.5 in the final refinement.[32]

Reaction of [Na][$C_{10}H_8$] and S_2N_2. A mixture of S_2N_2 (0.037 g, 0.40 mmol) and 15-crown-5 (0.176 g, 0.80 mmol) in 30 mL of THF was added to a dark green solution of [Na][$C_{10}H_8$] (0.121 g, 0.80 mmol) in 30 mL of THF at 23 °C ([Na][$C_{10}H_8$] was prepared by stirring 0.018 g of Na metal and 0.103 g of naphthalene in THF at 60 °C for 15 h). The dark red reaction mixture was stirred for 2 h. The solvent was evaporated under vacuum, and the resulting red, tarry product was washed with 2 × 10 mL of Et_2O giving a yellow powder (yield = 0.099 g, 97%, calculated as [Na(15-crown-5)][S_3N_3] (**1a**), see discussion). X-ray quality crystals of **1a** were obtained from THF after 1 h at −25 °C.

Reaction of [Na][Ph_2CO] and S_2N_2. A mixture of S_2N_2 (0.037 g, 0.40 mmol) and 15-crown-5 (0.176 g, 0.80 mmol) in 30 mL of Et_2O was added to a dark blue solution of [Na][Ph_2CO] (0.164 g, 0.80 mmol) in 30 mL of Et_2O at 23 °C ([Na][Ph_2CO] was prepared by stirring 0.018 g of Na metal and 0.146 g of benzophenone in Et_2O at 23 °C for 6 h). The reaction mixture was stirred for 2 h. The solvent was evaporated under vacuum, and the resulting orange-red, tarry product was washed with 2 × 10 mL of Et_2O giving a yellow powder (yield = 0.079 g, 77%, calculated as [Na(15-crown-5)][S_3N_3] (**1a**), see discussion). X-ray quality crystals of **1a** were obtained from THF after 1 h at −25 °C and identified by a unit cell determination.

Reaction of Cp_2Co and S_2N_2. A solution of Cp_2Co (0.151 g, 0.80 mmol) in 30 mL of THF was added to a solution of S_2N_2 (0.037 g, 0.40 mmol) in 40 mL of THF at −80 °C. The reaction mixture was allowed to reach room temperature (RT) in 2 h and it was stirred at 23 °C for 2 h. The resulting red powder was allowed to settle and the solvent was decanted via a cannula. The product was washed with 20 mL of THF followed by drying under a vacuum (yield = 0.078 g, 90% calculated as [Cp_2Co]-[S_3N_3] (**1b**), see discussion). X-ray quality crystals of **1b** were obtained from CH_3CN after 24 h at −25 °C.[33,34]

Results and Discussion

Voltammetry of S_2N_2. S_2N_2 was studied by CV in CH_3CN, CH_2Cl_2, and THF over scan rates of 0.05−20 V s^{-1} and temperatures of 20 ± 2 °C. Data for the CV responses of S_2N_2 in all three solvents are reported in Table 1 with potentials quoted relative to $Fc^{0/+}$. Representative CVs of S_2N_2 in CH_2Cl_2 at a scan rate of 0.2 V s^{-1} are shown in Figure 2. Two irreversible reduction processes appear upon sweeping the potential in the cathodic direction from the rest potential (−0.8 V vs $Fc^{0/+}$),

(25) (a) Boeré, R. T.; Roemmele, T. L. *Coord. Chem. Rev.* **2000**, *210*, 369. (b) Boeré, R. T.; Moock, K. H.; Parvez, M. *Z. Anorg. Allg. Chem.* **1994**, *620*, 1589.

(26) Weil, J. A.; Bolton, J. R.; Wertz, J. E. *Electron Paramagnetic Resonance*; John Wiley & Sons: New York, 1994.

(27) Duling, D. R. *J. Magn. Reson., Ser. B* **1994**, *104*, 105.

(28) (a) Rudolph, M. *J. Electroanal. Chem.* **2003**, *543*, 23. (b) Rudolph, M. J. *J. Electroanal. Chem.* **2004**, *571*, 289. (c) Rudolph, M. *J. Electroanal. Chem.* **2003**, *558*, 171. (d) Rudolph, M. *J. Comput. Chem.* **2005**, *26*, 619. (e) Rudolph, M. *J. Comput. Chem.* **2005**, *26*, 1193.

(29) Frisch, M. J.; Trucks, G. W.; Schlegel, H. B.; Scuseria, G. E.; Robb, M. A.; Cheeseman, J. R.; Montgomery, Jr., J. A.; Vreven, T.; Kudin, K. N.; Burant, J. C.; Millam, J. M.; Iyengar, S. S.; Tomasi, J.; Barone, V.; Mennucci, B.; Cossi, M.; Scalmani, G.; Rega, N.; Petersson, G. A.; Nakatsuji, H.; Hada, M.; Ehara, M.; Toyota, K.; Fukuda, R.; Hasegawa, J.; Ishida, M.; Nakajima, T.; Honda, Y.; Kitao, O.; Nakai, H.; Klene, M.; Li, X.; Knox, J. E.; Hratchian, H. P.; Cross, J. B.; Bakken, V.; Adamo, C.; Jaramillo, J.; Gomperts, R.; Stratmann, R. E.; Yazyev, O.; Austin, A. J.; Cammi, R.; Pomelli, C.; Ochterski, J. W.; Ayala, P. Y.; Morokuma, K.; Voth, G. A.; Salvador, P.; Dannenberg, J. J.; Zakrzewski, V. G.; Dapprich, S.; Daniels, A. D.; Strain, M. C.; Farkas, O.; Malick, D. K.; Rabuck, A. D.; Raghavachari, K.; Foresman, J. B.; Ortiz, J. V.; Cui, Q.; Baboul, A. G.; Clifford, S.; Cioslowski, J.; Stefanov, B. B.; Liu, G.; Liashenko, A.; Piskorz, P.; Komaromi, I.; Martin, R. L.; Fox, D. J.; Keith, T.; Al-Laham, M. A.; Peng, C. Y.; Nanayakkara, A.; Challacombe, M.; Gill, P. M. W.; Johnson, B.; Chen, W.; Wong, M. W.; Gonzalez, C.; and Pople, J. A.; *Gaussian 03*, Revision C.02; Gaussian, Inc.: Wallingford, CT, 2004.

(30) Sheldrick, G. M. *SHELXS-97, Program for Crystal Structure Determination*; University of Göttingen: Göttingen, Germany, 1997.

(31) Sheldrick, G. M. *SHELXL-97, Program for Crystal Structure Refinement*; University of Göttingen: Göttingen, Germany, 1997.

(32) Crystal data for **1a**: $C_{10}H_{20}N_3Na_1O_5S_3$, M_r = 381.46, orthorhombic, space group *Pnma*, a = 16.158(3), b = 14.383(3), c = 7.371(2) Å, V = 1713.1(6) Å^3, Z = 4, ρ_{calcd} = 1.479 g cm^{-3}, μ = 0.481 mm^{-1}, T = 173(2) K, 2809 reflections collected (θ range = 2.83−25.03°), 1557 unique (R_{int} = 0.0482), R_1 = 0.0546 [for 1018 reflections with $I > 2\sigma(I)$] and wR_2 = 0.1479 (for all data).

(33) The crystal structure of **1b** has been reported previously (ref 34) but the identification of the product of the S_2N_2/Cp_2Co reaction was confirmed by a full data collection and structure solution.

(34) Jagg, P. N.; Kelly, P. F.; Rzepa, H. S.; Williams, D. J.; Woollins, J. D.; Wylie, W. *J. Chem. Soc., Chem. Commun.* **1991**, 942.

Table 1. CV Data for S_2N_2 in CH_3CN, CH_2Cl_2, and THF and Calculated Enthalpies of Electron Attachment[a]

solvent	conc (mM)	E_p^{a1} (V)	E_p^{c1} (V)	E_n[b] (V)	E_p^{c2} (V)	E_p^{c3} (V)	E_p^{c4} (V)
CH_3CN	1.5	−0.26	−0.34	−0.30	−0.98	−1.40	−2.18
CH_3CN[c]				−0.28[d]		−1.23[d]	
CH_2Cl_2	2.0	−0.31	−0.38	−0.35	−1.02	−1.37	−2.20
THF	1.5	−0.29	−0.39	−0.34	−0.99	−1.29	−2.25
ΔH_{EA},[e] kJ mol^{-1}			−55		−204	−233	

[a] Obtained at a GC electrode at $\nu = 0.2$ V s^{-1} and $T = 20 \pm 2$ °C. [b] $E_n = [E_p^{a1} + E_p^{c1}]/2 \approx E^{o}_{(1)}$. [c] As reported in ref 16. Converted from the SCE scale to Fc by subtraction of 0.38 V (see ref 25). [d] Reported as $E_{p/2}$, i.e., the potentials at half-peak-height. [e] Calculated at the (U)B3LYP/6-311G++(3df,2dp)//(U)B3LYP/6-31G(d,p) level in Gaussian 03 (gas phase).

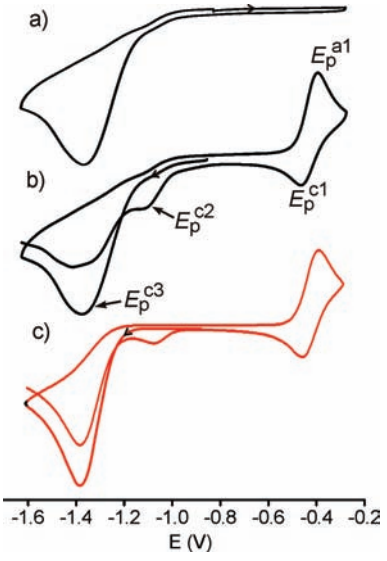

Figure 2. CVs (black lines) obtained on 2.0 mM solutions of S_2N_2 in CH_2Cl_2 containing 0.4 M [^{n}Bu$_4$N][PF$_6$] at a GC electrode at 20 °C, $\nu = 0.2$ V s^{-1} with the potential starting at −0.8 V: (a) sweeping in the positive direction and (b) sweeping in the negative direction. (c) Calculated CV (red line) resulting from input of the kinetic parameters listed in the text for the specific case of $\nu = 0.2$ V s^{-1} and $k_{f3} = 10^8$ M^{-1} s^{-1}, sweeping the potential first in the negative direction starting at −0.8 V.

designated as E_p^{c3} and E_p^{c4}, which are separated by approximately 0.8 V in all three solvents. E_p^{c3} appears at −1.37 V in CH_2Cl_2, −1.40 V in CH_3CN, and −1.29 V in THF. Further discussion will focus on voltammetry in CH_2Cl_2/0.4 M [^{n}Bu$_4$N][PF$_6$] which is the medium that we found to be the most versatile for this investigation; similar behavior occurred in the other two solvent/electrolyte systems. CVs obtained over an electrochemical window that was extended in the anodic direction show the absence of any additional processes when the initial sweep direction is anodic out to the solvent limit (Figure 2a), but the presence of a new redox process, E_p^{a1} at −0.31 V which has a return wave of lower peak current height, E_p^{c1} at −0.38 V ($\Delta E_p = 72$ mV) when the potential is first swept through the initial reduction process (Figure 2b). This indicates that the new process is likely to be the oxidation of a species generated from the decomposition of the product of electrochemical reduction at E_p^{c3}. Comparison of the peak potentials in CH_3CN with the earlier report of Banister and Hauptman[16] suggests that similar redox peaks were observed in their study. However, our extensive experience with the voltammetry[22] of S_4N_4 and the $[PPN]^+$ and $[Cp_2Co]^+$ salts of $[S_3N_3]^-$ allowed us to recognize the E_p^1 peaks immediately as those belonging to the $[S_3N_3]^{-/0}$ couple based on similarities in both the potentials and the I_p^{a1}/I_p^{c1} ratio rather than the previous assignment of this process to oxidation of S_2N_2.[16] As further confirmation of this assignment, a small peak designated as E_p^{c2} at −1.02 V appears subsequent to cycling through the $[S_3N_3]^{-/0}$ couple; such a process was anticipated based on our previous results and is unquestionably because of a small amount of S_4N_4 formed from the oxidation of $[S_3N_3]^-$ (see ref 22; this peak was reported previously at −1.06 V in CH_2Cl_2).

In view of the absence of E_p^{c2} in the initial cathodic scan (Figure 2a) we tentatively assign E_p^{c3} to the formation of $[S_2N_2]^{-\bullet}$. The behavior of this voltammetric peak when investigated over the full range of scan rates shows strong evidence of distortions that we attribute to adsorption on the electrode surface. For example, after several sequential scans, we observe a crossing over of the anodic and cathodic traces; cleaning the electrode surface by polishing then restores the signals to those observed originally (e.g., Figure 2a). Even scans on clean electrode surfaces show evidence of unusual peak shapes. This voltammetric indication that absorption seems to accompany E_p^{c3} is relevant to the SEEPR results (vide infra).

CVs extended further in the cathodic direction (Figure 3) show evidence of continuous current flow beyond E_p^{c3} with another identifiable peak (E_p^{c4}) at −2.2 V that has a peak current ~2/3 that of E_p^{c3}. While E_p^{c4} might be due to generation of the dianion $[S_2N_2]^{2-}$, its identification by voltammetric methods is unreliable. We chose instead to study this second process using a chemical approach (vide infra). Significantly, E_p^{c4} is not the same process as that observed from CV studies of solutions containing bulk S_4N_4, for which the (irreversible) second reduction peak is observed at the more anodic potential of −1.6 V versus $Fc^{0/+}$.[22]

Determination of the Diffusion Coefficient of S_2N_2. Both CV and RDE measurements on solutions of S_2N_2 were undertaken to determine the diffusion coefficient D.[35] The same approach was used as for the determination of D for S_4N_4 and $[S_3N_3]^-$.[22] CV measurements provided estimates of D of 8.16×10^{-6} cm^2 s^{-1} in CH_2Cl_2 and 7.65×10^{-6} cm^2 s^{-1} in CH_3CN. RDE measurements employed rotation rates between 1000−2250 rpm over a potential range of −0.6 to −2.2 V to a 2.1 mM solution of S_2N_2 in CH_2Cl_2. The Levich current (I_L) values were negatively affected by the electrochemical generation of $[S_4N_4]^{-\bullet}$ at rotation rates greater than 1000 rpm (Figure 4a). Therefore, all calculations had to take account of the number of moles of S_2N_2

(35) Bard, A. J.; Faulkner, L. R. *Electrochemical Methods: Fundamentals and Applications*, 2nd ed.; Wiley: New York, 2001.

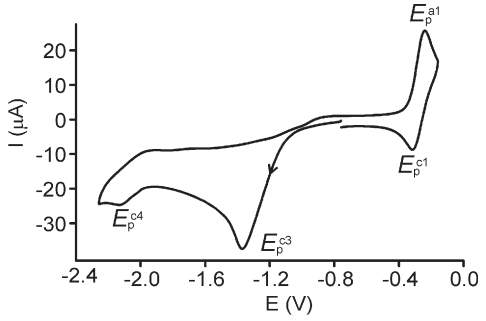

Figure 3. CV of a 2.0 mM soln of S_2N_2 in CH_2Cl_2 (0.4 M [^{n}Bu$_4$N][PF$_6$]), $\nu = 0.2$ V s^{-1}, $T = 20$ °C, with the potential sweep starting at −0.8 V and extending further negative to include the second reduction process at −2.3 V (labeled E_p^{c4}).

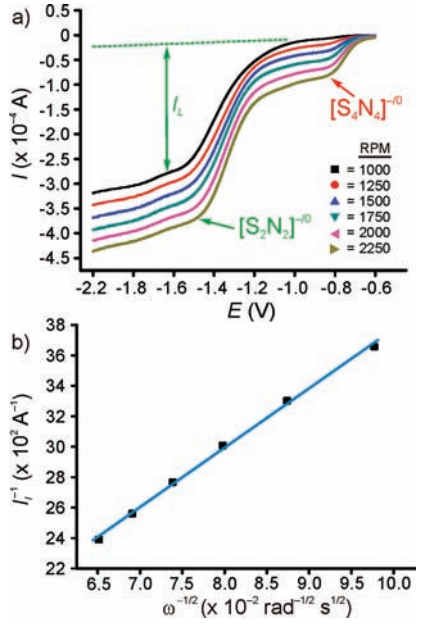

Figure 4. (a) RDE measurements on a 2.1 mM solution of S_2N_2 in CH_2Cl_2 with 0.4 M [^{n}Bu$_4$N][PF$_6$] at a 0.5 mm GC electrode, rotation rates = 1000−2250 rpm, $\nu = 0.010$ V s^{-1}; and (b) Koutecky−Levich[35] plot for the reduction of S_2N_2 ($R^2 = 0.998$) after correction for S_4N_4 formation (see text).

converted to $[S_4N_4]^{-\bullet}$ during the course of RDE measurements to obtain accurate I_L values. A plot of the reciprocal Levich current (I_L^{-1}) versus the reciprocal square root of the rotational velocity ($\omega^{-1/2}$) yielded a straight line (Figure 4b) with a slope = $(0.62nFAC\nu^{1/6}D^{2/3})^{-1}$.[35] Solving for D yielded a value of 8.73×10^{-6} cm^2 s^{-1}, in good agreement with the values obtained from CV measurements using the Randles−Sevcik equation.[35] Values for D based on both RDE and CV measurements are listed in Table 2. A best estimate for D used in modeling the voltammetric response of S_2N_2 (vide infra) was taken to be 9.13×10^{-6} cm^2 s^{-1}, the average of the values obtained by both CV and RDE methods in CH_2Cl_2. (Note that the diffusion coefficient of $[S_3N_3]^-$ is smaller by ∼50%, which accounts for the discrepancy in the peak currents (I_p^{a1} vs I_p^{c3}) for the two processes shown in Figure 2; for further background on such phenomena see ref 22.)

Digital Modeling of CVs of S_2N_2. To gain a better understanding of both the decay of $[S_2N_2]^{-\bullet}$ and the interconversion between S_2N_2, S_4N_4, and $[S_3N_3]^-$, we

Table 2. Diffusion Coefficient Values for S_2N_2 at $T = 21 \pm 2$ °C

solvent	electrode	RPM	D (S_2N_2)/10^{-6} cm^2 s^{-1}
		RDE[a]	
CH_2Cl_2	GC	2250	9.59[b]
CH_2Cl_2	GC	2000	9.44[b]
CH_2Cl_2	GC	1750	9.29[b]
CH_2Cl_2	GC	1500	9.20[b]
CH_2Cl_2	GC	1250	9.17[b]
CH_2Cl_2	GC	1000	9.30[b]
		RDE (Koutecky−Levich)	
CH_2Cl_2	GC		8.73[b]
		CV	
CH_2Cl_2[c]	GC		8.16[d]
CH_3CN[e]	GC		7.65[f]

[a] 0.4 M [^{n}Bu$_4$N][PF$_6$], $\nu = 0.01$ V s^{-1}. [b] 2.13 mM. [c] 0.4 M [^{n}Bu$_4$N][PF$_6$],], $\nu = 0.1$−1.0 V s^{-1}. [d] 2.00 mM. [e] 0.1 M [^{n}Bu$_4$N][PF$_6$],], $\nu = 0.1$−0.5 V s^{-1}. [f] 1.50 mM.

have built a model of the voltammetric behavior of S_2N_2 using DigiElch software.[28] Starting from the robust square scheme previously established from the excellent curve fitting simulations of CVs for the $S_4N_4 \leftrightarrow [S_3N_3]^-$ interconversion under the same conditions,[22] we developed a ladder scheme[36] in which the common parameters have the same meaning as in ref 22. (Scheme 1).[37] For the digital models, the scan rate ν was varied between 0.1−10 V s^{-1} and the shapes of the simulated CVs were compared to those measured experimentally. In this study it proved impossible to perform computerized line-fitting of the model to the experimental curves, most likely because of the abnormal peak shapes caused by adsorption (vide supra). However, reasonable visual fits were obtained over the full range of scan speeds (Figure 2c). Our model assumes a coupling reaction between the initially formed $[S_2N_2]^{-\bullet}$ with excess S_2N_2 in solution to form the known $[S_4N_4]^{-\bullet}$ (an EC mechanism with a second-order C step).[38] In view of the highly irreversible nature of the $[S_2N_2]^{-/0}$ redox couple, the value for $K_{eq\ 3}$ was set to be very large (10^6), rendering the C step irreversible regardless of scan rate. Values for k_{f3} which resulted in the greatest similarity between experimental and modeled CVs were $\geq 10^8$ M^{-1} s^{-1}, which converts to a half-life of $\leq 4 \times 10^{-6}$ seconds. Another feature of our model is that at faster scan rates (> 1 V s^{-1}), a return current peak occurs for the $[S_4N_4]^{-/0}$ redox couple which is not evident in the experimental CVs at similar scan rates. For the models to follow the experimental behavior over the full range of scan rates, k_{f1} values needed to be at least 25× greater than was observed previously,[22] that is,

(36) (a) Evans, D. H. *Chem. Rev.* **1990**, *90*, 739. (b) Evans, D. H. *Chem. Rev.* **2008**, *108*, 2113.

(37) Values for the kinetic parameters k_{s1}, k_{s2}, k_{f1}, and k_{f2} as well as the $E^{o\prime}$ values for each redox couple along with values for the working electrode area A (6.6×10^{-2} cm^2) and D ($S_4N_4/[S_4N_4]^{-\bullet} = 1.17 \times 10^{-5}$ cm^2 s^{-1}, $[S_3N_3]^-/[S_3N_3]^{\bullet} = 4.00 \times 10^{-6}$ cm^2 s^{-1}) were taken over from the previous study and initially held invariant (see ref 22). Other parameters employed were: $T = 22$ °C; concentration = 2×10^{-3} mol L^{-1}; $\nu = 0.1$−10 V s^{-1}; $R_u = 250\ \Omega$; $K_{eq\ 1} = K_{eq\ 3} = 10^6$; $K_{eq\ 2} = 1.804 \times 10^5$, D (S_2N_2, $[S_2N_2]^{-\bullet}$) = 9.13×10^{-6} cm^2 s^{-1}.

(38) For the EC and ECC classifications of heterogeneous electron transfer reactions (E) with coupled homogeneous chemical reactions (C), see chapter 12 of ref 35, pp. 471.

Scheme 1. Proposed "Ladder" Scheme Interrelating S_2N_2, $[S_4N_4]^{-\bullet}$ and $[S_3N_3]^-$[36]

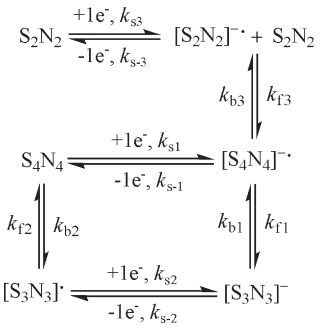

the half-life of $[S_4N_4]^{-\bullet}$ when in the presence of $[S_2N_2]^{-/0}$ appears to be significantly shorter than in bulk S_4N_4 solutions.[39] Final values for the adjustable parameters are as follows: $k_{s1} = 0.03\ cm\ s^{-1}$; $k_{s2} = 0.02\ cm\ s^{-1}$; $k_{s3} = 0.02\ cm\ s^{-1}$; $k_{f1} = 50\ s^{-1}$; $k_{f2} = 0.4\ s^{-1}$; $k_{f3} \geq 10^8\ M^{-1}\ s^{-1}$. This model thus predicts that the major product of the reduction of S_2N_2 in an aprotic environment will be $[S_3N_3]^-$ via the intermediate $[S_4N_4]^{-\bullet}$. This is fully supported by both EPR spectroscopic evidence and the results of chemical reduction, in which *quantitative* production of $[S_3N_3]^-$ salts is obtained (vide infra).

EPR Spectroscopy. To characterize the nature of the redox process occurring at E_p^{c3}, tentatively ascribed to a one-electron reduction of S_2N_2, we conducted SEEPR experiments on solutions of S_2N_2 in CH_2Cl_2, CH_3CN, and THF containing $[^nBu_4N][PF_6]$ as the supporting electrolyte. For these experiments, our newly developed low temperature solution electrochemical cell was used exclusively.[21,22] Temperatures were varied between −100 and −20 °C in CH_2Cl_2, −35 and 0 °C in CH_3CN, and −100 and 0 °C in THF. In practice, we found that in these systems accurate control of the electrolysis potentials was difficult. There is a strong tendency for over-reduction accompanied by adsorption of paramagnetic species exhibiting anisotropic EPR spectra onto the electrode surface (Figure 5). Significantly, both the isotropic (solution phase) and anisotropic (adsorbed) EPR signals decay rapidly even at low temperatures.

The most reliable results were obtained by using thin platinum or gold foil working electrodes and a Teflon-insulated silver wire reference electrode in CH_2Cl_2 solution at potentials that corresponded closely to E_p^{c3} as determined by RT voltammetry studies. When electrolysis is conducted at −1.4 V versus $Fc^{0/+}$ at temperatures between −90 °C and −40 °C, strong signals from $[S_4N_4]^{-\bullet}$ are obtained (Figure 5a; nine-line, $g = 2.0008(1)$, $a(N_{1-4}) = 0.115$ mT).[22] This spectroscopic result lends support to the mechanism whereby $[S_4N_4]^{-\bullet}$ is a direct and rapid product of the reduction of S_2N_2 (Scheme 1). Starting at −1.5 V and continuing to more negative potentials, the solution-phase spectrum of $[S_4N_4]^{-\bullet}$ begins to be replaced by an anisotropic spectrum, likely from species adsorbed onto the electrode surface. At −1.8 V, no solution-phase

(39) We tested this hypothesis during the EPR investigations by measuring the decay of the $[S_4N_4]^{-\bullet}$ signal when electrolysis was conducted at −1.0 V at −70 °C in a solution containing bulk S_2N_2. These measurements yielded a half-life for $[S_4N_4]^{-\bullet}$ in this environment of only 38 ± 1 s compared to an expected value of 280 ± 5 s based on the previous study (ref 22) on solutions containing pure S_4N_4.

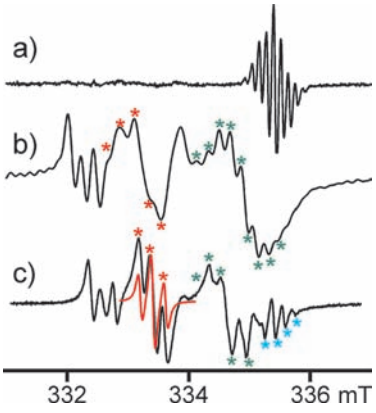

Figure 5. (a) Experimental first derivative EPR spectrum obtained during in situ reductive electrolysis at −1.4 V of S_2N_2 (82 s single scan) at a gold foil electrode at −70 °C in CH_2Cl_2 (0.4 M $[^nBu_4N][PF_6]$), 20.6 mM solution, modulation amplitude = 0.15 mT. (b) Spectrum obtained under identical conditions at −1.8 V. The g value of the apparent nine-line signal between 334.5 and 336 mT (green asterisks) is 2.0039(1). (c) Spectrum obtained at an intermediate potential for 99% $S_2{}^{15}N_2$. The red line is a simulation of the broadened three-line signal (red asterisks) for two equivalent ^{15}N nuclei with $a(^{15}N) = 0.20$ mT. Note that a little of the solution-phase $[S_4{}^{15}N_4]^{-\bullet}$ persists at the rhs of this spectrum (blue asterisks).

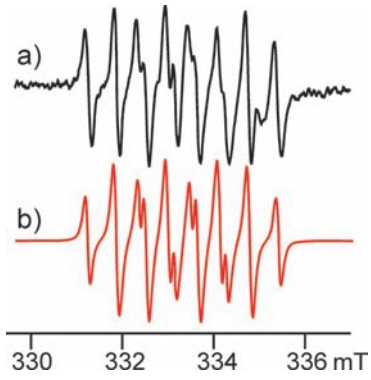

Figure 6. (a) Experimental EPR spectrum (black line) obtained during in situ reductive electrolysis of 1.5 mM S_2N_2 at −1.5 V (164 s single scan) at a platinum foil electrode in CH_3CN (0.1 M $[^nBu_4N][PF_6]$) at −20 °C after noise reduction, and (b) simulation (red line), with $a(^{14}N_1) = 1.12$ mT, $a(^{14}N_2) = 0.65$ mT, with $a(^1H) = 0.60$ mT, g value = 2.0136(1), mod. amp. = 0.2 mT.

signal remains (Figure 5b), but there appears to be a nine-line pattern at the right-hand side (green asterisks) that resembles solution-phase $[S_4N_4]^{-\bullet}$; however, the g value is different and the lines are broader than observed in solution at the same temperature. Similarly, the pattern between 333 and 334 mT (red asterisks) can be fit to a 1:2:3:2:1 quintet with hfs of 0.14 mT which could belong to $[S_2N_2]^{-\bullet}$. When identical experiments were performed with 99% isotopically labeled $S_2{}^{15}N_2$ (Figure 5c), the replacement of ^{14}N ($I = 1$) by ^{15}N ($I = 1/2$) results in the expected change in the fine structure of the EPR spectra from nine-line (green) and five-line (red) signals (Figure 5b) to five-line (green) and three-line (red) patterns. The ratio $a^{15}N{:}a^{14}N$ is about 1.4, as expected from the relative values of the nuclear gyromagnetic ratios. However, all the signals are shifted, albeit by a small amount, which is indicative of a species or species with anisotropic g tensors.[26] In view of this complexity, assignment of these signals to one or more specific

Table 3. Experimental and Calculated EPR Data for $[S_2N_2]^{-\bullet}$ and $[S_2N_2H]^{\bullet}$

species/condition	temp. (°C)	$a(N_1)$ (mT)	$a(N_2)$ (mT)	a(H) (mT)	LW (mT)	g value
$[S_2N_2]^{-\bullet}$/Calculated/*gas phase* [a]		0.52	0.52			
$[S_2N_2H]^{\bullet}/CH_3CN$ [b]	−20	1.12	0.65	0.60	0.090	2.0136(1) [e]
$[S_2N_2H]^{\bullet}/CH_3CN$ [b]	−30	1.12	0.64	0.64	0.093	2.0136(1) [e]
$[S_2N_2H]^{\bullet}/CH_3CN$ [b]	−35	1.12	0.63	0.69	0.090	2.0136(1) [e]
$[S_2N_2H]^{\bullet}$/mixture [c]	−20	1.11	0.69	0.71	0.078	2.0137(1) [e]
$[S_2N_2H]^{\bullet}$/mixture [c]	−50	1.10	0.70	0.75	0.081	2.0137(1) [e]
$[S_2N_2H]^{\bullet}$/acid [d]	−40	1.11	0.68	0.73	0.056	2.0142(1) [e]
$[S_2N_2H]^{\bullet}$/Calculated/*gas phase*[a]		0.88	−0.10	1.17		

[a] Computed at the UB3LYP/6-311G++(3df,3pd)//UB3LYP/6-31G(d,p) level with Gaussian03 (see text). [b] Containing 0.1 M $[^nBu_4N][PF_6]$. [c] 2/3 CH_2Cl_2, 1/3 *wet* CH_3CN containing 0.4 M $[^nBu_4N][PF_6]$. [d] CH_2Cl_2 containing 1 equiv. $HBF_4 \cdot 2OEt_2$ and 0.4 M $[^nBu_4N][PF_6]$. [e] Referenced internally to $[S_4N_4]^{-\bullet}$ at 2.0008(1) (ref 22.).

sulfur−nitrogen radicals is not warranted. Note that similar signals with rather small g anisotropy have been reported for intermediates in the preparation of the $(SN)_x$ polymer.[40]

In CH_3CN reductive electrolysis at −1.5 V at temperatures between −20 °C and −35 °C produced weak eight-line signals (Figure 6a). This spectrum is readily simulated by assuming coupling to two inequivalent nitrogen and single hydrogen atoms (Figure 6b), attributable to the neutral radical $[S_2N_2H]^{\bullet}$ through a proton transfer.[23] Significantly, the hfs values for N2 and H show significant variation with changes in temperature and environment (Table 3) as expected for a non-planar radical.[41] Since adventitious moisture is the most likely source of protons for forming $[S_2N_2H]^{\bullet}$, this radical was generated deliberately by electrolysis of "wet" 2:1 mixtures of CH_2Cl_2/CH_3CN (where the latter was degassed but not dried). The use of lower temperatures resulted in much stronger signals for $[S_2N_2H]^{\bullet}$ than obtained in CH_3CN (Table 3).

In an experiment designed to produce $[S_2N_2H]^{\bullet}$ via in situ electrochemical reduction of the protonated cation $[S_2N_2H]^+$, electrolysis of a solution of S_2N_2 in CH_2Cl_2/0.4 M $[^nBu_4N][PF_6]$ containing 1 equiv of $HBF_4 \cdot 2OEt_2$ was performed. At low temperatures, EPR spectra obtained from this solution resemble the signal for the absorbed species depicted in Figure 5b, but at higher temperatures the signals attributed to $[S_2N_2H]^{\bullet}$ grow in steadily until this is the dominant signal at −40 °C (Figure 7a, b).[42] Further warming to −20 °C resulted, after several minutes, in the generation of a persistent five-line signal (Figure 7c,d) that is readily attributed to $[S_3N_2]^{+\bullet}$ (g = 2.0111, a(N) = 0.31 mT).[43] This stable free radical is known to result from the treatment of either S_2N_2 or S_4N_4 solutions with strong acid.[43a,c] By contrast, the spectra obtained in wet CH_3CN at −20 °C show that the $[S_2N_2H]^{\bullet}$ signal in absence of strong acid decays with no indication of the formation of other EPR-active species. The EPR characterization of $[S_2N_2H]^{\bullet}$ provides strong support for the production of $[S_2N_2]^{-\bullet}$ in the one-electron electrochemical reduction of S_2N_2 associated with the voltammetric process at E_p^{c3}. The failure to observe $[S_2N_2]^{-\bullet}$ directly is attributed to the short lifetime of this radical in the presence of excess S_2N_2 as predicted by the voltammetric model (Scheme 1) and evidenced by spectroscopic observation of rapid and copious production of $[S_4N_4]^{-\bullet}$ from the main reaction.

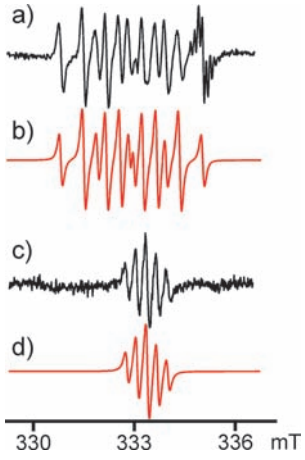

Figure 7. Experimental EPR spectra from single scans obtained during in situ reductive electrolysis of 1.5 mM S_2N_2 at −1.5 V (164 s single scan) at a platinum foil electrode in CH_2Cl_2 (0.4 M $[^nBu_4N][PF_6]$) containing $HBF_4 \cdot 2OEt_2$: (a) at −40 °C (black line) and (b) the simulation of this spectrum (red line); note that in the simulation the small contribution by $[S_4N_4]^{-\bullet}$ (14% by area) has been omitted to more clearly show the high-field line component. (c) At −20 °C after about 10 min (black line). (d) Simulation (red line) of the spectrum in (c).

DFT Calculations. The $[S_2N_2H]^{\bullet}$ neutral radical is calculated at the UB3LYP/6-31G(d,p) level of theory to adopt a slightly butterfly ring geometry in the gas phase (dihedral angle between SNS planes of 6.9°) with the hydrogen atom lying out of the ring plane (Figure 8; see figure and legend for metric parameters). The calculated hfs constants of $a(N_1)$ = 0.88 mT, $a(N_2)$ = −0.10 mT, and a(H) = 1.17 mT are in reasonable agreement with the experimental values (Table 3). The geometry of $[S_2N_2]^{-\bullet}$

(40) The solid-state EPR spectrum of the unstable "red monomer" obtained as a side-product from the preparation of S_2N_2, measured at −118 C°, has considerable similarity to the adsorbed species in this work, though it is not identical. (a) Love, P.; Myer, G.; Kao, H. I.; Labes, M. M.; Junker, W. R.; Elbaum, C. *Ann. N.Y. Acad. Sci.* **1978**, *313*, 745. (b) Love, P.; Labes, M. M. *J. Chem. Phys.* **1979**, *70*, 5147.

(41) (a) See ref 26, p 260 ff. (b) Kaim, W.; Bock, H.; Nöth, H. *Chem. Ber.* **1978**, *111*, 3276. (c) Alberti, A; Benaglia, M; DellaBona, M. A.; Guerra, M; Hudson, A; Macciantelli, D. *Res. Chem. Intermed.* **1996**, *22*, 381. (d) Ingold, K. U.; Nonhebel, D. C.; Walton, J. C. *J. Phys. Chem.* **1986**, *90*, 2859.

(42) EPR signal decay measurements from spectra obtained at −70 °C for peaks attributed to $[S_2N_2H]^{\bullet}$ fit best to a first-order decay process, with an estimated half-life of 7 ± 1 s. Thus, the lifetime of $[S_2N_2H]^{\bullet}$ is about 5 × shorter than that of $[S_4N_4]^{-\bullet}$ under the same conditions (see ref 39).

(43) (a) Chapman, D.; Massey, A. G. *Trans. Faraday Soc.* **1962**, *58*, 1291. (b) Gillespie, R. J.; Kent, J. P.; Sawyer, J. F. *Inorg. Chem.* **1981**, *20*, 3784. (c) Preston, K .F.; Sutcliffe, L. H. *Magn. Reson. Chem.* **1990**, *28*, 189; note that in (a) this radical is misidentified as $[S_2N_2]^{+\bullet}$. (d) One of the referees pointed out that the $[S_3N_2]^{+\bullet}$ radical cation is a logical product of the reduction in an acidic environment of $[S_3N_2]NH_2^+$ (with loss of NH_4^+); this cation is a known product of the reaction of HBF_4 with $[S_3N_3]^-$ salts: Marcellus, C. G.; Oakley, R. T.; Cordes, A. W.; Pennington, W. T. *Can. J. Chem.* **1984**, *62*, 1822.

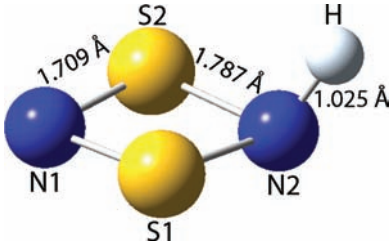

Figure 8. Optimized gas-phase UB3LYP/6-31G(d,p) structure of $[S_2N_2H]^{\bullet}$; ∠S1−N1−S2 94.7°, ∠N1−S1−N2 87.8°, ∠S2−N2−S1 89.4°, ∠S1−N2−H 108.9°, ∠N1−N2−H 120.4°, S1N1S2−S1N2S2 dihedral 6.9°.

at this same level of theory is close to that previously calculated using a specialized basis set.[15]

DFT calculations were also undertaken to determine the enthalpies of electron attachment of S_2N_2, S_3N_3, and S_4N_4 in the gas phase to rationalize the measured redox potentials in solution (Table 1). The calculations show that in the gas phase, ΔH_{EA} $S_3N_3 > S_4N_4 > S_2N_2$, that is, the same trend as the redox potentials in solution. An important consequence is that the solution electron transfer reaction (eq 1) is predicted to be non-spontaneous.[36]

$$[S_4N_4]^{-\bullet} + S_2N_2 \rightarrow S_4N_4 + [S_2N_2]^{-\bullet} \qquad E^\circ = -0.35\ \text{V} \qquad (1)$$

This reaction would seem to be a necessary component of the proposed catalytic cycle for the rapid conversion of solutions of S_2N_2 to S_4N_4 with just a small amount of reducing agent.[14,44]

Chemical Reduction of S_2N_2: Synthesis and Crystal Structure of [Na(15-crown-5)][S_3N_3]. The electrochemical experiments described above were complemented by investigations of the chemical reduction of S_2N_2 with the primary objective of determining the possible production of the dianion $[S_2N_2]^{2-}$, a potential alternative source of the short-lived radical anion $[S_2N_2]^{-\bullet}$ via one-electron oxidation. These reactions were conducted with three reagents that display increasing strength for reduction (formal potential vs $Fc^{0/+}$): Cp_2Co (−1.33 V in CH_2Cl_2), $[Ph_2CO]^{-\bullet}$ (−2.30 V in THF), and $[C_{10}H_8]^{-\bullet}$ (−3.10 V in THF).[45] The formal potentials of the first two reducing agents are close to the measured values for E_p^{c3} and E_p^{c4}, respectively, while the naphthalenide radical anion is a significantly stronger reducing agent than E_p^{c4} (vide supra).

The reactions were performed in a 2:1 molar ratio by using the sodium salts of radical anions ($[Ph_2CO]^{-\bullet}$ and $[C_{10}H_8]^{-\bullet}$) in the presence of 15-crown-5 and cobaltocene Cp_2Co. The products were identified by X-ray crystallography, which revealed that in all three reactions, despite the various strengths of the reducing agents,

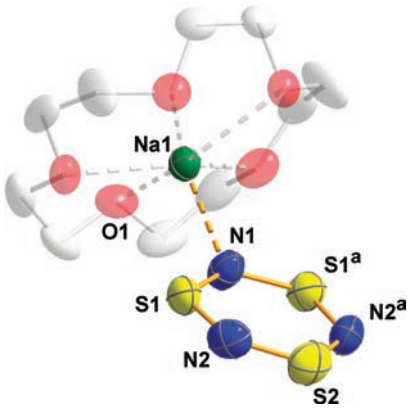

Figure 9. Crystal structure of **1a** with the atomic numbering scheme. Hydrogen atoms have been omitted for clarity. [a] Symmetry operation: x, $0.5 - y$, z.

Scheme 2. Formation of the $[S_3N_3]^-$ Anion from Chemical Reduction of S_2N_2

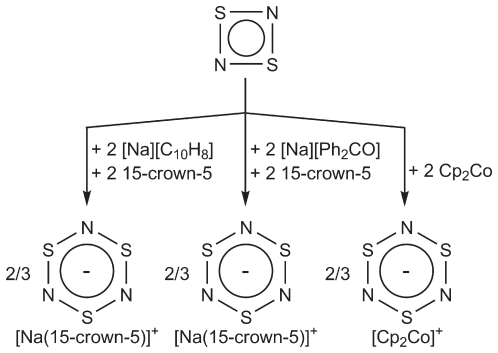

formation of the known $[S_3N_3]^-$ monoanion as $[Cp_2Co]^+$ and $[Na(15\text{-crown-5})]^+$ salts in excellent yields occurred (Scheme 2). The voltammetry and EPR results revealed the rapid conversion of $[S_2N_2]^{-\bullet}$ to $[S_4N_4]^{-\bullet}$ and subsequently, $[S_3N_3]^-$. Thus, the outcome of the chemical reductions is consistent with the observations made for the electrochemical reduction of S_2N_2, even in the presence of an excess of reducing agent. Consistent with previous attempts to generate the $[S_2N_2]^{2-}$ dianion by deprotonation of $[S_2N_2H]^-$,[20a] no evidence for the formation of the $[S_2N_2]^{2-}$ dianion was garnered from either the chemical or the electrochemical reductions.

The crystal structure of $[Cp_2Co][S_3N_3]$, obtained from the reduction of S_4N_4, has been reported previously.[34] However, [Na(15-crown-5)][S_3N_3] (**1a**) is the first structurally characterized alkali-metal salt of $[S_3N_3]^-$. A large, non-coordinating cation is usually required to stabilize the six-membered ring; simple alkali-metal salts of $[S_3N_3]^-$ are explosive in the solid state.[46] As illustrated in Figure 9, the crystal structure of **1a** shows a C_s-symmetry with the O1, Na1, N1, and S2 atoms in the mirror plane. The Na^+ cation, coordinated by the crown ether, displays a fairly strong Na···N interaction of 2.388(5) Å (cf. for example Na···N of 2.375(3) and

(44) For a catalytic cycle to operate (albeit slowly) it is only necessary that a small amount of $[S_2N_2]^{-\bullet}$ forms in eq 1 for turnover to be possible. Since voltammetry under quiescent conditions is not a good test for what happens in the bulk, we attempted to address this issue by performing punctuated electrolysis in stirred solution, halting after 1, 10, and 50% of the required current had passed, waiting for a catalytic reaction to transpire and interrogating the mixture via RDE voltammetry. However, our results were inconclusive probably because of equipment limitations. Testing of the catalytic hypothesis by chemical or electrochemical approaches is left for future work.

(45) Connelly, N. G.; Geiger, W. E. *Chem. Rev.* **1996**, *96*, 877.

(46) Bojes, J.; Chivers, T. *Inorg. Chem.* **1978**, *17*, 318.

(47) (a) Nöth, H.; Warchhold, M. *Eur. J. Inorg. Chem.* **2004**, 1115. (b) Ikorskii, V. N.; Irtegova, I. G.; Lork, E.; Makarov, A. Y.; Mews, R.; Ovcharenko, V. I.; Zibarev, A. *Eur. J. Inorg. Chem.* **2006**, 3061.

Table 4. Selected Bond Lengths (Å) and Bond Angles (deg) in **1a** and Other $[S_3N_3]^-$ Salts[a,b]

	1a	1b[d]	1c	1d	1e	1f	1g
N1−S1	1.617(2)	1.623	1.587(4)	1.623(4)	1.615(5)	1.604(12)	1.641(9)
N1−S1[c]	1.617(2)	1.623	1.603(3)	1.616(4)	1.630(5)	1.609(12)	1.601(9)
N2−S1	1.607(4)	1.625	1.597(4)	1.564(4)	1.616(6)	1.626(12)	1.566(8)
N2−S2	1.605(4)	1.618	1.615(3)	1.636(4)	1.646(5)	1.584(12)	1.628(8)
N2[c]−S2	1.605(4)	1.618	1.590(4)	1.630(4)	1.605(6)	1.599(12)	1.590(7)
N2[c]−S1[c]	1.607(4)	1.625	1.593(4)	1.574(4)	1.632(6)	1.580(12)	1.609(7)
Na1···N1	2.388(5)						
S1−N1−S1[c]	124.4(3)	123.7	124.9(3)	122.6(2)	123.8(3)	122.9(8)	122.6(5)
S1−N2−S2	124.1(2)	123.4	122.9(2)	125.2(3)	124.2(3)	122.6(8)	124.3(5)
S2−N2[c]−S1[c]	124.1(2)	123.4	124.9(2)	125.5(3)	123.2(4)	124.2(8)	124.4(5)
N1−S1−N2	115.3(2)	116.7	116.2(2)	116.7(2)	117.5(3)	116.5(7)	116.6(4)
N2−S2−N2[c]	116.4(3)	116.1	116.1(2)	113.4(2)	115.4(3)	117.0(7)	115.6(4)
N2[c]−S1[c]−N1	115.3(2)	116.7	114.8(2)	116.1(2)	115.5(3)	116.5(7)	116.4(4)

[a] Atomic numbering scheme of **1b-1g** has been changed to match that in **1a**. [b] (**1a**) $[Na(15\text{-crown-5})]^+$, (**1b**) $[Cp_2Co]^+$,[34] (**1c**) $[(PhCN_2S_2)_2Cl]^+$,[49] (**1d**) $[PhCN_2S_2]^+$,[49] (**1e**) $[PPN]^+$,[22] (**1f**) $[^nBu_4N]^+$,[50] (**1g**) $[Ph_4P]^+$.[19b] [c] Symmetry operation in **1a**: x, 0.5-y, z. [d] Values taken from the cif-file deposited in the Cambridge Crystallographic Data Center.

2.393(5) Å in [Na(18-crown-6)(THF)$_2$][NCS] and [Na(15-crown-5)][NCS],[47a] respectively). The most germane comparison with **1a**, perhaps, is the salt [Na(15-crown-5)]-$[SN_2C_2N_2S]$ containing a heterocyclic C,N,S radical anion, in which the Na−N distances are 2.511 and 2.837 Å.[47b] The larger values in the latter salt are likely attributable to its infinite chain arrangement of N···· Na^+···N···· Na^+ contacts, whereas the $[S_3N_3]^-$ salt has a single N···· Na^+ contact on one side of the crown. The six-membered $[S_3N_3]^-$ ring in **1a** shows a slight, albeit almost negligible, distortion toward a chair conformation with the maximum deviation from planarity of 0.023(3) Å. All the bond lengths and angles at S and N atoms, respectively, are equal within experimental errors (Table 4). The bond parameters are also comparable to the average values of 1.61 Å (S−N), 124° (∠SNS) and 116° (∠NSN) observed in the previously reported salts of the $[S_3N_3]^-$ anion (Table 4). The only notable intermolecular close contacts in **1a** are the two N···H connections of 2.700(4) and 2.703(4) Å involving the N2 (and by symmetry N2[a]) atom and the adjacent crown ether (cf. sum of the van der Waals radii for nitrogen and hydrogen 2.74 Å).[48]

Comparison of the solid-state structures of $[S_3N_3]^-$ salts demonstrates that the subtle distortion in the six-membered ring is surprisingly independent of the cation−anion interactions. The diversity in the anion bond parameters in **1c** and **1d** ($[(PhCN_2S_2)_2Cl]^+$ and $[PhCN_2S_2]^+$ salts, respectively) was attributed mainly to interionic S···S interactions,[49] and in **1e** ($[PPN]^+$) to the strong hydrogen-bonding with the MeOH solvate.[22] On the other hand, there are no close contacts, even to the hydrogen atoms of the cations, in the $[^nBu_4N]^+$ (**1f**)[50] and $[Ph_4P]^+$ (**1g**)[19b] salts, but significant distortions in the S−N bond lengths are also observed in these salts. Curiously, structures **1a** and **1b** display no significant variation in the bond parameters, despite the presence of strong interionic Na···N (**1a**) and N···H interactions in **1b**. We note that, unlike **1c-1g**, the $[S_3N_3]^-$ anion in **1a** and **1b** exhibits crystallographic mirror symmetry. In summary, the 10 π-electron $[S_3N_3]^-$ anion[8c] exhibits minor distortions from regular D_{3h} symmetry in the solid state that are not consistently determined by anion−cation interactions.

Conclusions

Both electrochemical and chemical reduction of S_2N_2 produce the $[S_3N_3]^-$ anion. The former process can be modeled by a mechanism in which the initially formed $[S_2N_2]^{-\bullet}$ radical anion reacts with excess S_2N_2 to afford $[S_4N_4]^{-\bullet}$, verifying a literature prediction.[14] The latter species is known to decay rapidly to give $[S_3N_3]^-$.[22] In the presence of a proton donor EPR spectra indicate that trapping of $[S_2N_2]^{-\bullet}$ occurs to form the neutral radical $[S_2N_2H]^{\bullet}$, which was identified by simulation of the EPR spectrum as supported by DFT calculations. Consistent with the results of previous chemical approaches,[20] our investigations of the reduction of S_2N_2 provided no evidence for the formation of the dianion $[S_2N_2]^{2-}$.

Acknowledgment. The authors gratefully acknowledge financial support from the Natural Sciences and Engineering Research Council (Canada), the Alberta Ingenuity Fund (T.L.R.) and the University of Lethbridge for the potentiostat. We also wish to express our indebtedness to Prof. R. T. Oakley (University of Waterloo) for providing advice and the apparatus for the synthesis of S_2N_2. The referees are thanked for helpful insights and suggestions.

Supporting Information Available: X-ray crystallographic file in CIF format. This material is available free of charge via the Internet at http://pubs.acs.org.

(48) Pauling, L. *The Nature of the Chemical Bond*, 3rd ed.; Cornell University Press: Ithaca, NY, 1960.

(49) (a) Banister, A. J.; Clegg, W.; Hauptman, Z. V.; Luke, A. W.; Wait, S. T. *J. Chem. Soc., Chem. Commun.* **1989**, 351. (b) Banister, A. J.; Hansford, M. I.; Hauptman, Z. V.; Luke, A. W.; Wait, S. T.; Clegg, W.; Jorgensen, K. A. *J. Chem. Soc., Dalton Trans.* **1990**, 2793.

(50) Bojes, J.; Chivers, T.; Laidlaw, W. G.; Trsic, M. *J. Am. Chem. Soc.* **1979**, *101*, 4517.